scientific reports

Check for updates

OPEN

An innovative chitosan-coated aquatic feed pellets production from coastal waste using top-spray fluidized bed drying

Jatuphat Maikaew[1], Naruebodee Srisang[1]✉, Supreeda Tambunlertchai[2] & Siriwan Srisang[1]

Coastal wastes such as crab shells, shrimp shells, and seaweed are rich in proteins, lipids, and bioactive compounds, making them valuable raw materials for aquafeed production. In this work, three aquatic feed pellets were developed and tested under different drying temperatures from 70 to 110 °C to evaluate the pellet durability index (PDI), specific energy consumption in water removal (SEW), and nutrient quality. The formulation containing high crab shell content showed the most balanced nutritional profile but required further improvement in mechanical strength. To address this, chitosan coating was applied using a top-spray fluidized bed system, with process conditions optimized through response surface methodology (RSM). The RSM demonstrated the optimal coating condition at a concentration of about 1.25% (w/v), a spray rate of about 32.5 mL/min, and a temperature of about 110 °C, with the lowest of drying time (DT) and specific energy consumption (SEC). The optimized coating significantly improved PDI and water solubility index while preserving nutritional balance. It also enhanced antimicrobial properties, which are desirable for feed storage. Microscopic and structural analyses confirmed good adhesion of the coating. Overall, this study demonstrates a sustainable pathway to convert coastal waste into high-quality aquafeed, offering both environmental benefits and practical value for aquaculture industries.

Keywords Aquatic feed pellets, Chitosan coating, Top-spray fluidized bed technique, Coastal waste, Response surface methodology

Sustainable aquaculture (i.e., aquafeed and innovation) plays a critical role in research due to the growing global demand for sustainable fish farming as an alternative to traditional fish-meal-based feeds[1]. In 2021, Thailand generated about 24.98 million tons of municipal solid waste accounted for 38.76% of total waste, as reported by the Pollution Control Department (PCD) in Thailand. This high proportion highlights the potential for food and organic waste valorization. Recent strategies emphasize the circular economy and local waste valorization, particularly in coastal areas with enormous amounts of waste such as seaweed, shrimp, and crab shells. These wastes can be recycled into animal feed due to the large amounts of nutrients, including protein, fat, and carbohydrates, contained in shrimp and crab shells[2]. Pattanaik, et al.[3] reported that the protein and high antioxidant activity from crustacean shell waste can be utilized as a good feed ingredient in animal diets. Seaweed serves as a source of essential nutrients, including proteins and lipids, thereby contributing to its nutritional and functional value in feed formulations[4]. *Spirulina* has been selected as an alternative high-quality protein source to fish meal, particularly due to its contribution to the sustainability of the aquafeed industry. Zhang, et al.[5] reported that *Spirulina* was employed to replace fish meal, resulting in improved growth performance in fish. Mamun, et al.[6] demonstrated that *Spirulina platensis* was more effective at concentrations exceeding 7.5% of fish meal, resulting in a higher specific growth rate compared to diets without the *Spirulina*. Several studies have investigated the survival, growth rate, and digestibility in terms of the shrimp shell and *Spirulina*[7]. On the other hand, the crab shell was evaluated to determine whether essential substances used in animal feed, such as chitosan[8], calcium[9], and chitin[10]. These studies demonstrated the possibility for sustainable aquafeed production from coastal waste. However, the aquafeed was still prepared using traditional production techniques, which may have an impact when different methods are employed to improve the process or product quality.

[1]Department of Engineering, King Mongkut's Institute of Technology Ladkrabang, Prince of Chumphon Campus, Chumphon 86160, Thailand. [2]National Nanotechnology Center (NANOTEC), National Science and Technology Development Agency (NSTDA), Pathum Thani 12120, Thailand. ✉email: naruebodee.sr@kmitl.ac.th

The ingredients used in AFP production, including crab shell, shrimp shell, and *Spirulina*, are processed into pellets to improve their transportation stability and storage efficiency. The AFP has a high moisture content, as water is a critical component in the pelletization process[11]. Drying is a fundamental process used to reduce the water content of feed materials, thereby lowering water activity, improving long-term storage stability, and reducing transportation costs. Conventional drying techniques commonly applied in AFP production include oven drying[11], belt drying[12], and convective drying[13], each with different levels of efficiency and energy consumption. For example, Carmen, et al.[14] reported that oven drying of shrimp-waste feed reached equilibrium moisture in 180 min at 50 °C, making it the slowest method, whereas fluidized-bed drying combined with infrared heating required only 8 min to achieve similar moisture levels. Innovative drying technologies have therefore gained attention for improving heat and mass transfer rates. Fluidized-bed drying assisted by a halogen lamp (FBH) is one such hybrid technique, in which near-infrared radiation enhances internal heat penetration and accelerates moisture removal[15]. This system is particularly effective for granular and pelletized materials due to its uniform bed distribution. In addition to drying, coating processes are widely used to enhance product quality[16]. Chaabani, et al.[17] demonstrated that vacuum-coating conditions influence both processing time and final trout-feed properties. Among advanced coating and drying technologies, the top-spray fluidized bed technique (TFT) is an advanced drying–coating system in which air suspends the particles while a liquid coating is sprayed from the top, allowing simultaneous moisture removal and uniform deposition of coating materials. Junka and Rattanamechaiskul[18] presented that the TFT coated with zinc oxide nanoparticles on the paddy surface can inhibit fungus, improve product quality, and reduce processing time to minimize moisture loss.

Chitosan has been recognized as an effective coating agent due to its ability to enhance antioxidant activity, suppress fungal growth, promote growth performance, and stimulate digestive enzyme activity[19,20]. Its application is particularly well-suited for the AFP products requiring extended shelf life. While many studies have focused on the development of advanced pelletizing machines and process parameters for the AFP[21], relatively few have addressed the integration of efficient drying and coating techniques. This study proposes the use of TFT to improve the drying and coating processes in AFP production. Nonetheless, the TFT application in chitosan-coated AFP has been scantily investigated. Response surface methodology (RSM) is a widely used statistical technique for modeling and optimizing processing conditions in various food and feed applications, such as drying and coating processes[22,23].

Therefore, this study aimed to develop the innovative AFP production in drying and coating processes using coastal waste, i.e., shrimp shells, crab shells, and seaweed. The preliminary AFP identification was performed under different conditions of formulations and air temperatures. It was evaluated in terms of pellet durability index (PDI), specific energy consumption in water removal (SEW), and nutritional value. After that, the AFP was improved in quality using a chitosan coating via TFT, and the optimal conditions in the coating process were determined, i.e., the chitosan concentration (Cc), spray rate (Sr), and temperature (T), using the RSM. The optimal AFP characteristics after coating were examined in the microstructure (SEM), composition (XRD), physical and mechanical properties, and antimicrobial properties.

Materials and methods

AFP recipes

Figure 1 shows the coastal wastes after grinding, i.e., shrimp (*Litopenaeus vannamei* species), crab shells (*Scylla* species), and seaweed (*Spirulina*). The *Spirulina* was a high-protein source (≈ 44%)[24], which was obtained from the Chlorella Plus shop (Chumphon, Thailand), and it was fixed at 80 g/kg within the ingredient. These feedstock amounts were investigated to replace the minced fish meat in the traditional recipe, and these feedstocks were divided into three recipes (A, B, and C) as shown in Table 1. Each recipe, approximately 1 kg in weight, was provided to the AFP with a diameter of 3.75 mm and a length of 6.60 mm, as shown in Fig. 2. The AFP from three recipes were compared with the original recipe which consisted of rice bran (200 g/kg), fish oil (50 g/kg), corn flour (50 g/kg), binder (50 g/kg), minced fish meat (500 g/kg), and water (150 g/kg), as according to Srisang, et al.[25]. The AFP was dried using the FBH at drying temperatures of 70, 90, and 110 °C combined with the halogen lamp (1000 W).

Effect of the mixture and drying temperature on AFP characteristics

The effect of mixture and drying temperature parameters on AFP characteristics was investigated in terms of minimum fluidization velocity (m/s), drying kinetics, specific energy consumption during water removal (kWh/kg_{H2O}), pellet durability index (%), and nutritional content (%).

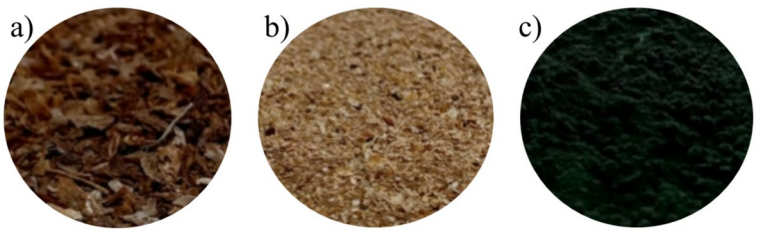

Fig. 1. Feedstocks: (a) shrimp shells, (b) crab shells, and (c) seaweeds.

Mixture type	Ingredient content (g/kg)		
	A	B	C
Shrimp shells	140	210	280
Crab shells	280	210	140
Seaweeds	80	80	80
Rice Bran	100	100	100
Fish oil	60	60	60
Wheat flour	150	150	150
Binder	50	50	50
Total vitamins	20	20	20
Water	120	120	120

Table 1. Ingredients in AFP recipes.

Fig. 2. Aquatic feed pellets (AFP).

Minimum fluidization velocity
The AFP amount (≈ 2 kg) was fed to a drying chamber with a bed height of 11 cm. The fluidization velocity and pressure (Pa) within the drying chamber were measured using a Testo model 510 (Germany). Both values were plotted in a correlated graph to find the minimum fluidization velocity.

Drying kinetics
Drying kinetics were evaluated at three experimental temperatures: 70, 90, and 110 ˚C. During each drying run, the moisture content (MC) of the AFP was measured every 5 min. To determine the dry mass (w_d) required for calculating MC on a dry basis, a separate oven-drying step was performed according to the AOAC (2000) method. In this step, the samples were dried in hot-air oven at 104 ˚C oven-drying procedure was used only for determining dry mass and was not part of the drying kinetics experiment. Before each experiment, the AFP samples were weighed to obtain the initial wet weight (w_w). The MC under each drying condition was expressed on a dry-basis percentage (% d.b.) using Eq. (1).

$$\mathrm{MC}\ (\%\ \mathrm{d.b.}) = ((w_w - w_d)/w_d) \times 100 \quad (1)$$

where:
w_w = weight of wet sample (g). w_d = weight of dry sample (g).
The moisture reduction rate (MRR) from initial to final moisture content was determined for each drying condition using a modified version of Srisang, et al.[15], as presented in Eq. (2):

$$\mathrm{MRR}\ (\%\ \mathrm{d.b./min}) = ((M_{in} - M_{final})/\mathrm{drying\ time\ (min)}) \times 100 \quad (2)$$

where:
M_{in} = Initial moisture content (% d.b.). M_{final} = Final moisture content (% d.b.).

Specific energy consumption in water removal
Specific energy consumption in water removal (SEW) was used to evaluate the energy efficiency of different AFP drying and coating conditions. The SEW represented the amount of energy required to remove one kilogram of water from the sample and was calculated according to the adapted method described by Ao, et al.[26], as shown in Eq. (3):

$$SEW(kWh/kg_{H_2O}) = \frac{Q_{total}}{M_{we}} \quad (3)$$

where:

Q_{total} = The total of electrical energy consumption (kWh). M_{we} = The water removal during drying (kg).

The drying system consisted of separate heating units for each experimental temperature. The equipment included a 1000 W halogen lamp, a 1072.12 W blower, and individual electric heaters operating at 1258.82 W (70 °C), 1297.28 W (90 °C), and 1311.83 W (110 °C).

Pellet durability index (PDI)

The PDI examination method was modified from de Cruz, et al.[27]. The samples were prepared at approximately 150 g (P_b) and placed in a test kit according to the standard ASAE S269.4; then, the test kit was rotated at 50 rpm for 10 min. The remaining AFP samples in the test kit were shaken through a 3.4 mm mesh-sized sieve for 1 min. The AFP weight within the sieve (P_a) was recorded, and the PDI was calculated according to Eq. (4):

$$PDI = \left(\frac{P_a}{P_b}\right) \times 100 \quad (4)$$

Nutrition content

The nutrient quantities within AFP were measured for protein, fat, and fiber using AOAC (2019) 981.10, AOAC (2019) 920.39, and AOAC (2019) 978.10 methods, respectively.

The AFP coating via the top-spray fluidized bed technique (TFT)

A TFT was performed as accorded with the report of Maikawe, et al.[28]. Figure 3 shows a schematic diagram of the top-spray fluidized bed coater, which consists of two main parts: a fluidized bed and spraying parts. A fluidized bed part comprised of a stainless-steel coating chamber with an inner diameter of 0.2 m and a height of 0.5 m. A blower with a blade size of 0.3 × 0.09 m pushed the air into the coating chamber, controlled by a 2 HP motor and the inverter (Fuji Electric, Thailand). The Testo model 510 differential pressure meters (Germany) measured the air velocity and pressure drop. The inlet air was heated using a heater and a 1000 W halogen lamp. The hot air entered the bed through the distributor plate, a stainless-steel plate with a 3 mm diameter hole. In the spraying part, the solution pump (Model CNPB 0705, Prominent, Germany) was used to supply the coating solution to the two-fluid nozzle (Model 1/4J series, Spraying Systems Co., Wheaton, IL, USA). The nozzle installed above the distributor plate is approximately 23 cm in length. The air compressors (Tiger air compressors, model TGA33-150 M, China) provided air atomization for spraying.

Coating material and preparation

The coating material was chitosan (medium molecular weight and deacetylated chitin) purchased from Sigma-Aldrich, China. Acetic acid (glacial) 100% (M = 60.05 g/mol). The chitosan powder was dissolved in water at a concentration of 0.5–2% (w/v), which served as the solvent for acetic acid at a concentration of 1% (v/v). The mixture was then stirred overnight using a hotplate magnetic stirrer at room temperature, with a magnetic bar velocity of 820 rpm.

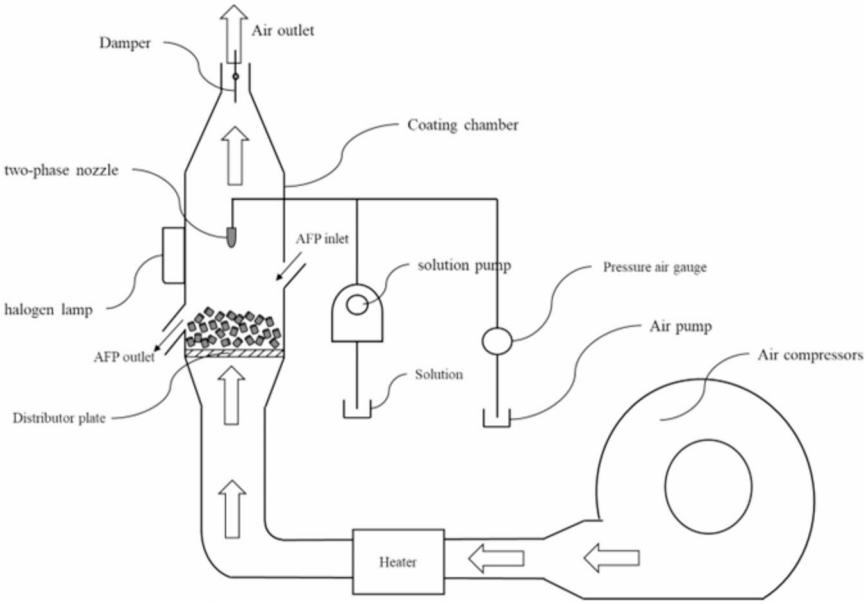

Fig. 3. Schematic diagram of top-spray fluidized bed coater.

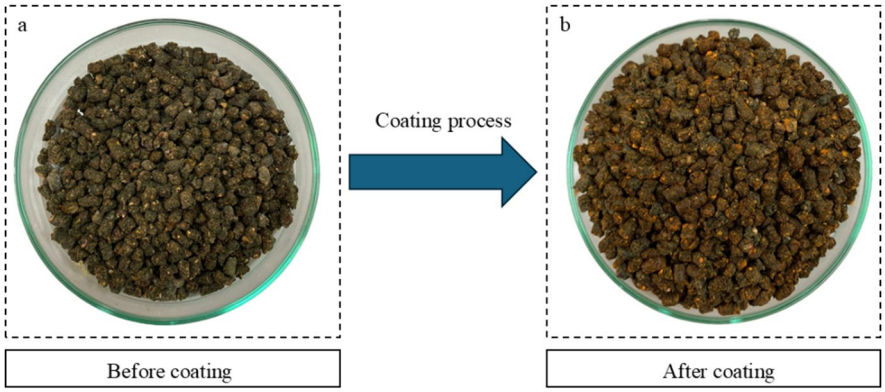

Fig. 4. Uniform coating appearance of AFP: (a) uncoated sample and (b) chitosan-coated sample.

Variable	Units	Symbols	Levels of factor		
			-1	0	1
Concentration of chitosan	% w/v	Cc	0.5	1.25	2
Spray rate	mL/min	Sr	32.5	48.75	65
Temperature	°C	T	70	90	110

Table 2. Level of factor and symbol of the independent variable.

Coating procedure

Approximately 2 kg of AFP were loaded into the coating chamber for each run. The samples were fluidized to ensure continuous particle movement during coating. The chitosan solution was sprayed at 32.5–65 mL/min for 15 min under an atomization pressure of 4 bar. The fluidization air (70–110 °C) enabled uniform particle suspension, which facilitated homogenous coating coverage. Coating uniformity was visually confirmed by the consistent red color of the AFP surface, and no aggregation or uneven deposition was observed, as shown in Fig. 4. After coating, the AFP samples were stored at 4 °C for further analysis.

Response surface methodology (RSM)

Response surface methodology (RSM) is a well-established statistical design and optimization technique commonly applied in the various processes, such as food, feed, drying, and coating processes. In the present study, RSM was employed to model the relationship between among processing variables and to identify the optimal conditions for AFP coating using TFT. The RSM was displayed in Eq. (5) with a cubic polynomial model; the independent variable (X) comprised the chitosan concentration (Cc substituted with X_1), spray rate (Sr substituted with X_2), and temperature (T substituted with X_3); the response variable (Y_i) was drying time (DT) and specific energy consumption (SEC); the regression coefficient substituted with b symbol in Eq. (5):

$$Y_i = b_0 + b_1X_1 + b_2X_2 + b_3X_3 + b_{11}X_1^2 + b_{22}X_2^2 + b_{33}X_3^2 + b_{12}X_1X_2 + b_{13}X_1X_3 + b_{23}X_2X_3 \quad (5)$$

where b_0 is a constant and the coefficients in Eq. (5) are linear (b_1, b_2, b_3), quadratic (b_{11}, b_{12}, b_{13}), and interaction (b_{12}, b_{13}, b_{23}). A Box-Behnken design (BBD) with three variables and three levels of each factor is presented in Table 2. The BBD consisted of 12 runs at -1, 0, and 1 level for three variables and 3 replications at the center point (run numbers of 13,14, and 15), as represented in Table 3.

The statistical significance of the models was examined through regression analysis using Minitab, version 20.1. The lack of fit should be more than 0.05, indicating the models could explain the change in the experimental domain. The coefficient of determination (R^2) and adjusted determination $\left(R^2_{adj}\right)$ suggested that the model could explain the relation between the two variables.

Specific energy consumption in coating production (SEC)

The SEC considered electrical energy consumption in the coated process, based on the production yield, due to the significant energy usage in air heating, halogen lamps, blowers, air compressors, and solution pumps. The SEC was calculated using the adapted equation Srisang, et al.[15], as shown in Eq. (6):

$$\text{SEC} = \text{EEC}/\text{Amount of AFP} \quad (6)$$

where:

EEC = The sum of electrical energy consumption (kWh). Amount of AFP = The amount of coated AFP (kg).

Run No	Experimental conditions		
	Cc	Sr	T
1	0.5	32.5	90
2	2	32.5	90
3	0.5	65	90
4	2	65	90
5	0.5	48.75	70
6	2	48.75	70
7	0.5	48.75	110
8	2	48.75	110
9	1.25	32.5	70
10	1.25	65	70
11	1.25	32.5	110
12	1.25	65	110
13	1.25	48.75	90
14	1.25	48.75	90
15	1.25	48.75	90

Table 3. Levels and code numbers of the independent variable.

Optimal coating process

Response variables were considered desirable because the lowest DT and SEC values indicate an increasing efficiency of production and sustainability in reducing greenhouse gas emissions. The optimal coating process was identified through the desirability functions, which serve as a multi-response optimization methodology[29]. The desirability value should approach 1, indicating the suitable desired value of response, calculating the following Eq. (7):

$$D = \sqrt[w]{d_1 \times d_2 \times \ldots \times d_i} \tag{7}$$

where D was the composite desirability, w was the weights assigned to individual responses based on their relative importance, and d_i was a desirability index from individual responses.

AFP characteristics after coating

All AFP samples were examined for characteristics in terms of PDI, water solubility index, nutrition content, microstructure, composition change, and inhibition zone.

Microstructure

The microstructure was analyzed using a Scanning Electron Microscope (SEM) and Energy Dispersive X-ray Spectrometer – SEM-EDS (6610LV, JEOL Ltd., Tokyo, Japan). The surface and cross-section of AFP were photographed using an accelerating voltage of 15 kV with the magnification of 25X and 300X, respectively.

X-ray diffraction pattern (XRD)

The XRD analysis was used to investigate the composition change within AFP. The XRD data were collected using an X-ray diffractometer (Bruker AXS, Model D8 Discover, Germany) equipped with a Cu source at 40 kV and 40 mA. Each XRD profile was obtained using a scanning rate of 0.02°/min over a 2θ angle range of 10 to 60°.

Water solubility index (WSI)

WSI analysis adapted from the method of Wang, et al.[30]. The AFP samples were placed in mesh 5 g (m_1) and then transferred to a beaker containing 500 mL of water, with a depth of 5.5 cm. The magnetic bar was stirred and vibrated for 20 min at room temperature. The soaked AFP was dried at a temperature of 135 °C for 2 h, and its weight (m_2) was measured. The WSI was calculated using Eq. (8):

$$WSI = \frac{m_1 \times [(1-x) - m_2]}{m_1 \times (1-x)} \times 100 \tag{8}$$

where:

x = The amount of water before drying, expressed as a decimal, was measured using the standard AOAC 193.01: 2000 method.

Inhibition zone

Antifungal testing of the coated AFP was performed using inhibition zone analysis, modified from the method described by Jain, et al.[31]. The potato dextrose agar (PDA) and fungus food were prepared. The *Aspergillus spp.* were subcultured at a concentration of 10^5 spores/mL, quantified using a Neubauer chamber grid (Boeco,

Germany). Subsequently, a 10 mL aliquot of the fungal suspension was inoculated onto potato dextrose agar (PDA) supplemented with the AFP-coated optimal process. The culture was incubated at 30 °C for intervals of 3, 5, and 7 days, during which the diameter of the clear zone was systematically measured.

Statistical analysis

SEC, PDI, and WSI were measured in triplicate per condition. These data were statistically analyzed using a one-way ANOVA with Tukey's B post hoc method in SPSS (Version 29, IBM Corp.). The RSM used the Minitab program (version 19) to design the experimental conditions, and the MATLAB program (version R2019b) was used to plot the surface and control graphs.

Results and discussion

AFP characteristics from the different recipes and drying temperatures

The fluidized bed velocity has been measured in relation to the superficial air velocity and the pressure drop. Figure 5 illustrates the relationship between pressure drop and superficial air velocity, where the pressure increases continuously with air velocity between 2 and 9 m/s. The highest pressure drops, 450 Pa, occurred at a superficial air velocity of 9.8 m/s, indicating that this air velocity was the minimum fluidization velocity of the AFP at 2 kg; this air velocity was insufficient for dispersion throughout the bed in the fluidization state. When the air velocity increased by more than 9.8 m/s, the pressure drop decreased because the lift force from the air overcame the particle's weight. Thus, the minimum fluidization velocity was multiplied by 1.1 to obtain a suitable velocity for fluidization, resulting in 10.78 m/s.

Figure 6 shows the change in moisture content at different drying temperatures (70, 90, and 110 °C) using the FBH technique, as exhibited in Fig. 6a and b, and 6c, respectively. The initial moisture content of the AFP from each recipe (i.e., A, B, and C recipes) was similar, at approximately 35.81 ± 0.58%, 34.87 ± 0.15%, and 34.49 ± 0.69% (d.b.), respectively. This high moisture content may facilitate the growth of fungi. The moisture content in every condition was quickly diminished during the primary drying duration (0–5 min) due to moisture removal from the AFP surface via evaporation. The drying kinetics of AFP showed a clear dependence on drying temperature. As the drying temperature increased from 70 to 90 and 110 °C, the moisture content of AFP decreased more rapidly. This trend was particularly evident during the initial drying period (5 min). At 70 °C, the moisture content decreased to approximately 21–25% (d.b.), whereas at 90 °C and 110 °C, a more pronounced reduction was observed, with moisture contents of approximately 18–20% and 16–19% (d.b.), respectively. This behavior indicates that higher drying temperatures enhance the moisture removal rate, especially at the early stage of drying, due to the increased driving force for heat and mass transfer. Then, the moisture gradually decreased, caused by slower diffusion from inside the AFP to the surface. These altered moisture patterns were observed in the fluidized bed drying[15]. Figure 6a and c exhibit the abatement of moisture content in the A, B, and C recipes at drying temperatures of 70 and 110 °C within 25 min; the A recipe had the final moisture content in the range of 2.76–8.56% (d.b.) which was higher than the B recipe (2.31–6.09% (d.b.)) and C recipe (2.16–7.28% (d.b.)). Furthermore, the equilibrium moisture content, defined as the final stable moisture level of the samples, was determined for each drying condition, as shown in Table 4. Although the numerical values of MRR increased with drying temperature (110 °C > 90 °C > 70 °C), the differences were not statistically significant ($p > 0.05$), as shown in Table 5. This indicates that, while higher temperature tends to accelerate moisture removal, the variability within the measurements resulted in non-significant differences among the treatments. The moisture reduction in the A recipe was slower than in the B and C recipes at a drying temperature of 70 °C, which was

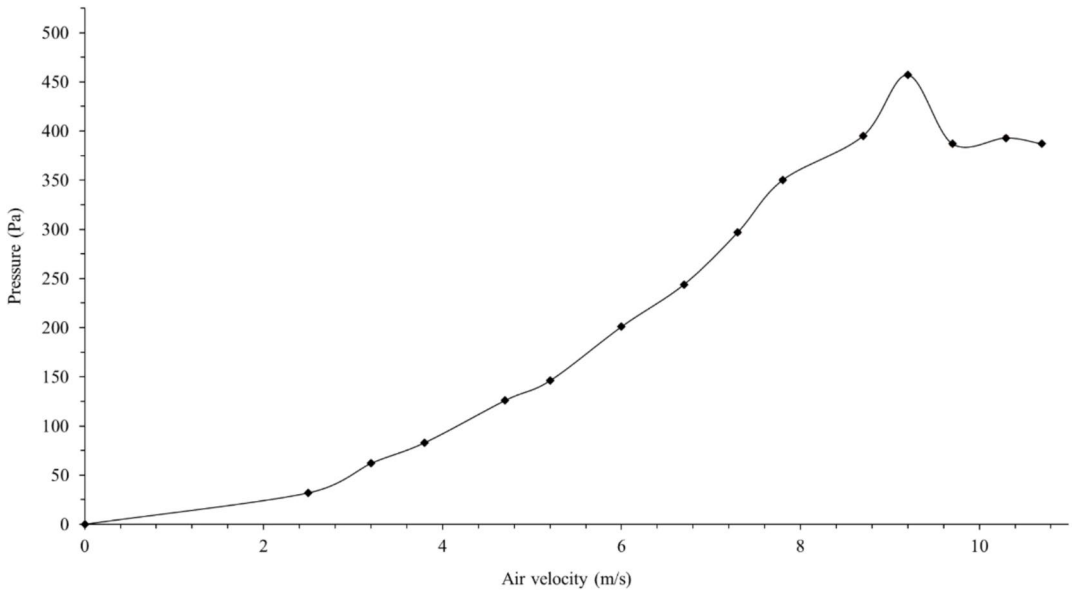

Fig. 5. Minimum fluidized bed velocity of AFP.

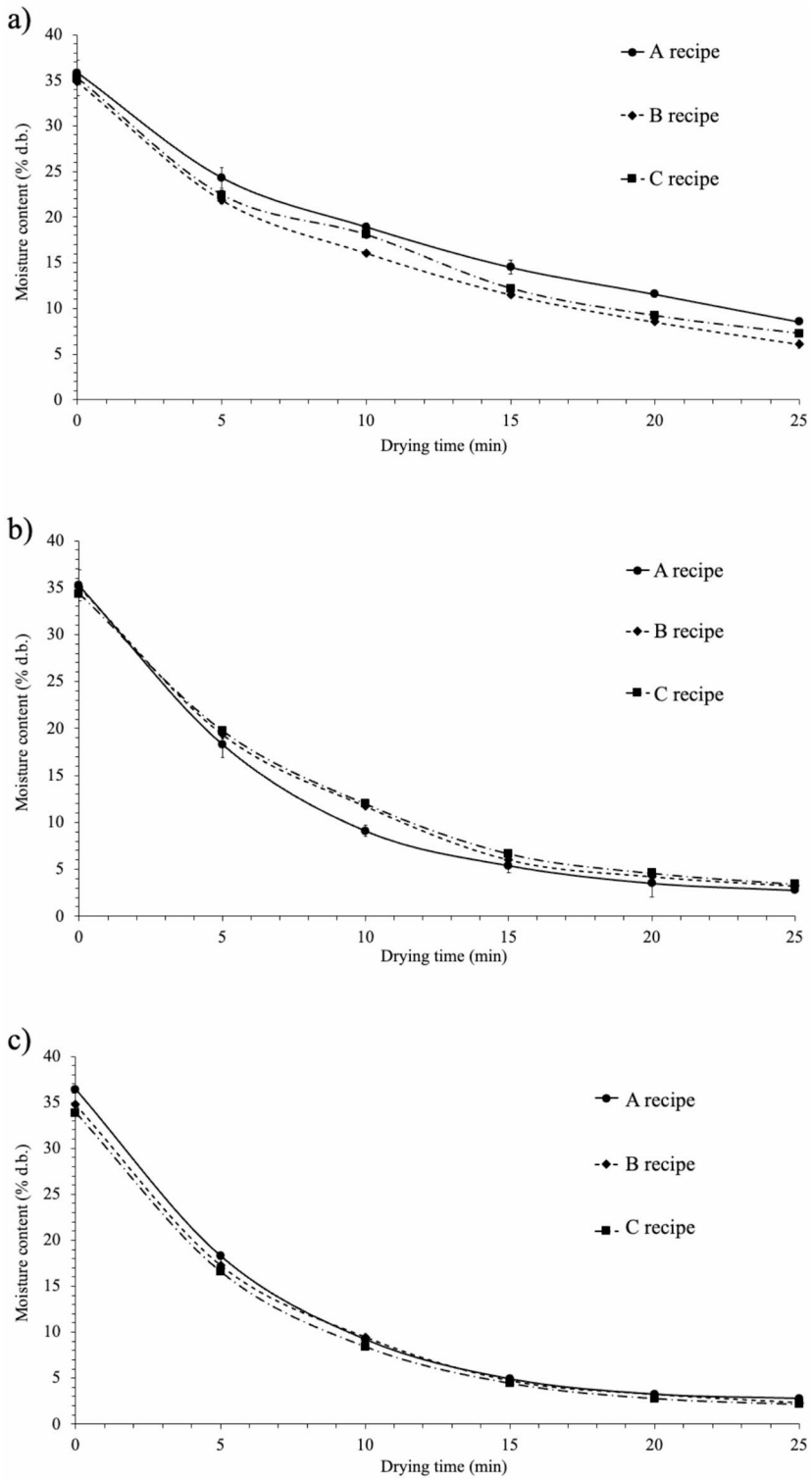

Fig. 6. Drying kinetics of the AFP in A recipe, B recipe, and C recipe at a drying temperature of (a) 70, (b) 90, and (c) 110 °C.

evident because the lower drying temperature provided less energy for water removal. This effect was attributed to the high content of crab shells. Crab shells are richer in chitin, thicker, and harder, properties that restrict water diffusion during drying[32]. As a result, the A recipe exhibited a lower drying temperature and a slower reduction of moisture content. Nonetheless, the drying kinetics of A, B, and C recipes showed little contrast when the drying temperature was increased to 110 °C, especially at post-drying times of 10 min. These results implied that the different AFP recipes did not affect the drying kinetics of AFP's moisture when the moisture was

	A	B	C
70 ˚C	8.56 ± 0.1	6.09 ± 0.52	7.28 ± 0.18
90 ˚C	2.75 ± 0.17	3.25 ± 0.02	3.43 ± 0.11
110 ˚C	2.76 ± 0.19	2.31 ± 0.07	2.16 ± 0.13

Table 4. The equilibrium moisture content for each drying condition.

Recipe	70 °C (% d.b./min)	90 °C(% d.b./min)	110 °C(% d.b./min)
A	$108.96 \pm 0.97^{a,*}$	$129.92 \pm 6.04^{bc,*}$	$134.55 \pm 1.03^{c,*}$
B	$114.86 \pm 2.47^{a,*}$	$127.14 \pm 0.93^{bc,*}$	$129.79 \pm 0.72^{bc,**}$
C	$111.85 \pm 7.17^{a,*}$	$123.7 \pm 0.92^{b,*}$	$126.84 \pm 0.7^{bc,***}$

Table 5. MRR analysis in each recipe and drying temperatures. Mean with different scripts (a, b, c) in the same row are significantly different ($p \leq 0.05$), while means with different scripts (*, **, ***) in the same column are significantly different ($p \leq 0.05$).

rapidly decreased using the high drying temperature. Remarkably, the drying kinetics at a drying temperature of 90 °C as shown in Fig. 6b, the moisture content rapidly diminished in A recipe as compared with B and C recipe which resulted in the final moisture content was 2.75 ± 0.17% (d.b.) and was lower than B recipe (3.25 ± 0.02% (d.b.)) and C recipe (3.43 ± 0.11% (d.b.)). The results showed that increasing the drying temperature enhanced moisture removal from AFP, which can be attributed to the softening of chitinous structures and increased vapor–pressure gradients at elevated temperatures. At 70 °C, recipes B and C exhibited faster moisture reduction than recipe A, likely due to the porous structure of shrimp shells that promotes early-stage moisture release. However, at higher drying temperatures (≥ 90 °C), the lipids present in shrimp shells began to melt and redistribute on the AFP surface, forming a thin hydrophobic layer that inhibited moisture diffusion. Cyprian, et al.[33] similarly reported that samples with higher lipid content experienced slower drying rates because lipids act as a physical barrier that restricts heat transfer and surface moisture migration. This mechanism explains why recipes B and containing higher shrimp shell content showed reduced moisture diffusivity at temperatures above 90 °C. Although B and C recipes showed a slower moisture reduction as compared to the A recipe, they exhibited lower water activity, which contributed to prolonged storage. Thus, the drying kinetics at temperatures of 90 and 110 °C in every recipe had significantly more slopes than at 70 °C, which corresponded with the higher MRR as presented in Table 5. The A recipe at the drying temperature of 110 °C exhibited the highest MRR value, which was significantly greater than those obtained under other conditions. The MRR increased significantly with temperature, which aligns with the findings of Srisang, et al.[15], who reported that the moisture reduction rate (MRR) varied substantially with drying temperature and heating method, the present study also shows that the drying temperature and the inherent composition of the material influence the rate of moisture removal. Similar trends were observed in our study, where the 110 °C condition yielded the highest MRR (Table 5), consistent with established drying theory. However, every drying temperature in this study prepared the final moisture content of AFP at the desirable level of about lower than 12%[34]. The FBH technique required approximately 10 min of drying time to achieve the desirable moisture content, whereas traditional tray drying in aquatic feed production took more than 6 h to reduce the moisture content to 12% (d.b.)[35]. Therefore, the FBH could reduce the drying time by approximately 5 h and 50 min.

Figure 7 displays the specific energy consumption in water removal (SEW) of the AFP for the distinct conditions of AFP recipes and drying temperatures. The A recipe had the highest SEW (≈ 2.81 ± 0.02 kWh/kg_{H2O}) at a drying temperature of 70 ˚C due to the lowest MRR value, as shown in Table 5. The SEW value at 70 °C was significantly more than the other drying temperatures in every AFP recipe. In contrast, the SEW value in each recipe at the drying temperatures of 90 and 110 °C did not essentially diverge. The SEW values in each recipe demonstrated a declining tendency as the drying temperature increased; these trends aligned with the elevated MRR and resulted in reduced energy consumption. The varied AFP recipe had an insignificant effect on the SEW value under a similar drying temperature. The drying temperature of 110 °C yielded the lowest SEW, corresponding with the high MRR values, which provided the shortest drying time to achieve the target moisture content. Le, et al.[36] reported that high drying temperatures resulted in low energy consumption; they suggested that hybrid drying technology could reduce energy consumption. Nanvakenari, et al.[37] demonstrated that the drying temperature mainly influenced the specific energy consumption in the drying process SEC, with the higher temperatures resulting in lower SEC values. Furthermore, the FBH technique was a hybrid drying method that could rapidly evaporate water at the surface of the AFP using hot air, while also penetrating the inside of the AFP with near-infrared radiation, resulting in fast water removal and energy savings.

Figure 8 represents the pellet durability index (PDI) of dried AFP from each condition, evaluating physical integrity, which indicates that the AFP retains its form under vibration. The PDI value insignificantly diverged in each AFP recipe under the same drying temperature, except for the C recipe at 110 °C, due to the influence of the severe drying temperature, which resulted in an inferior structure. The trend of PDI value in almost all recipes declined with increasing drying temperature, due to the inverse correlation between PDI and temperature. The higher drying temperatures in A and B recipes tended to reduce PDI values, particularly at the extreme

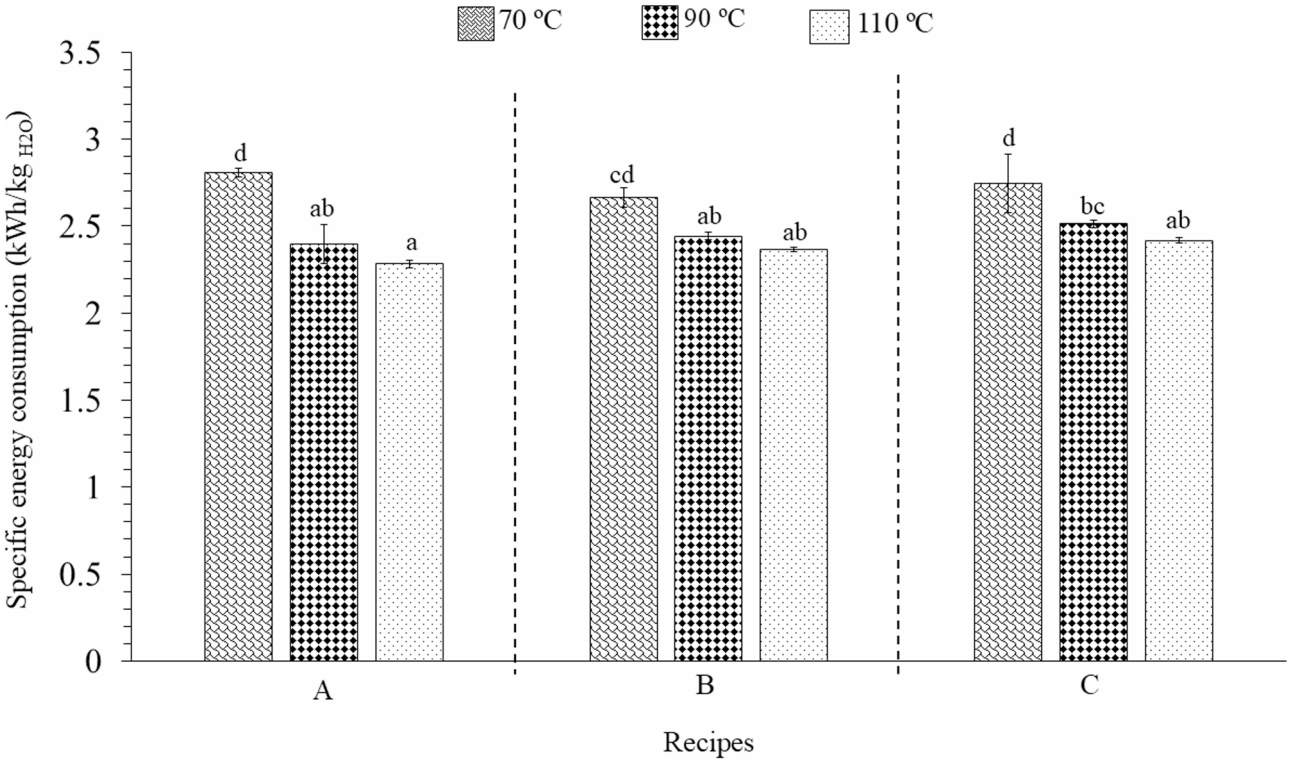

Fig. 7. Specific energy consumption in water removal of the AFP from the different recipes and drying temperatures. a.b, c,d Different superscripts are significantly different at $p \leq 0.05$.

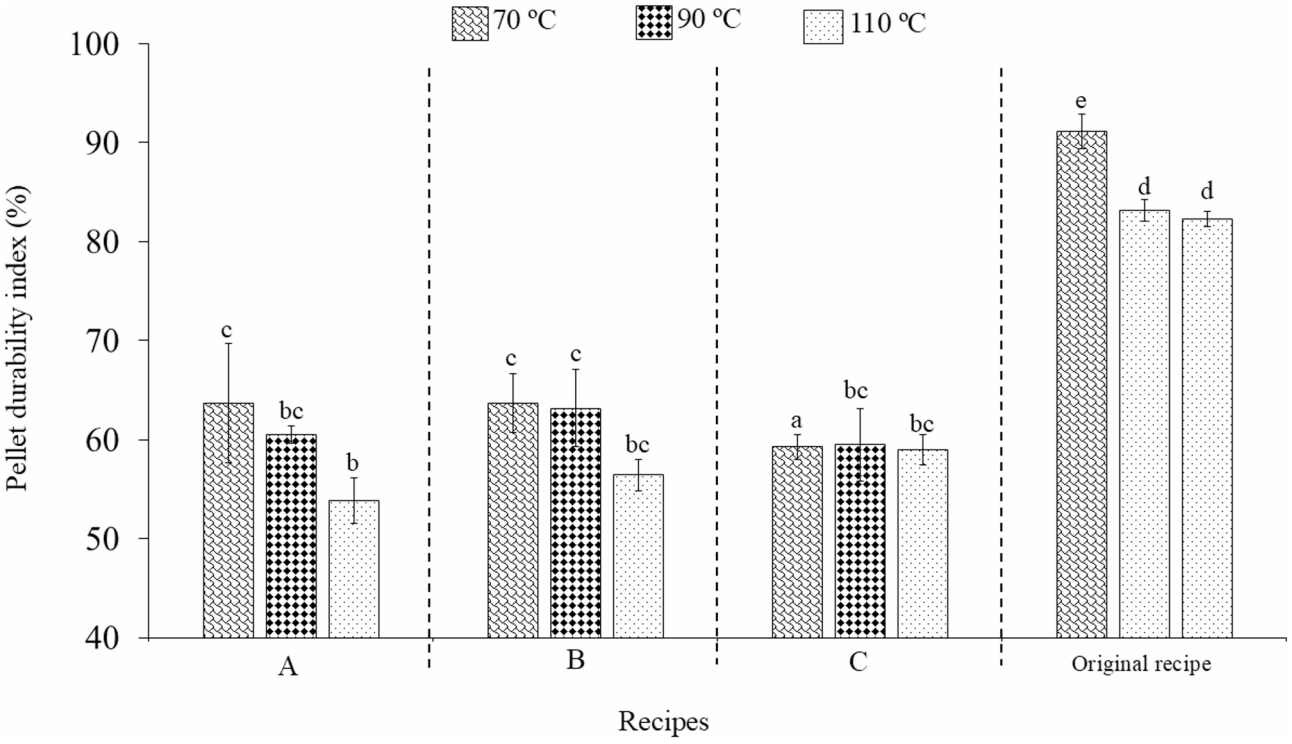

Fig. 8. Pellet durability index of the AFP from the different recipes and drying temperatures. a, b,c, d,e Different superscripts are significantly different at $p \leq 0.05$.

temperature of 110 °C in the A recipe, where the PDI dropped to approximately 53.8%. The A recipe had the highest PDI (63.71%) at a drying temperature of 70 °C. These results indicated that PDI was inversely related to MRR, with the highest MRR values corresponding to the lowest PDI. As a result, fast water evaporation from inside pellets affected looser structures[38] and resulted in the augmented pore amount within the structure. The C recipe nearly showed a PDI value of about 59% at every drying temperature; this result stemmed from the higher shrimp shell content within the ingredient, which resulted in a less cohesive texture and led to poor homogeneity after the pelletizing and drying process. In the same way, at a drying temperature of 70 °C, the C recipe exhibited a significantly lower PDI value than the A recipe, likely due to its more shrimp shell content. At all tested drying temperatures (70, 90, and 110 °C), the original recipe demonstrated superior PDI values compared to A recipes through C, achieving 91.17, 83.16, and 82.26%, respectively, as shown in Fig. 8. Although fish meal shares a powder-like texture with shrimp and crab shells, it tends to mix more homogeneously due to its more cohesive characteristics. Mostafa, et al.[39] noted the poor pelletization, which resulted in a lower PDI value. The mixture characteristics were a crucial factor affecting AFP quality, as the PDI value was expected to exceed 70%[40].

The nutrient content is crucial because it is essential for aquaculture, particularly in terms of fish growth performance[41]. The AFP recipes at a drying temperature of 110 °C were selected to investigate the nutrient content because this condition provided the lowest SEC, which indicated high energy efficiency. The AFP recipes in this research gave high protein (≈ 33–37%) and lipid (≈ 9–11%) as shown in Table 6 because there were seaweeds about 8% in the mixture, which were the main protein and lipid sources[24]. The C recipe had the minimum protein (≈ 33%) and lipid (≈ 9%) contents. The A recipe had the maximum protein (≈ 37%) and lipid (≈ 11%) contents, while the original recipe, which used fish meal in a mixture, had the lower protein (≈ 26%) and lipid (≈ 5%) content. As a result, the A recipe had more crab shell content than the C recipe, which tended to increase the total protein and lipid contents. Liu, et al.[42] reported that the protein content in shrimp shells was approximately 7.98%. Jeon and Yeom[43] pointed out that the protein content in crab shells was approximately 12%. These findings demonstrated that the protein content in crab shells is higher than in shrimp shells. The crude fiber content in AFP should be the least (not exceeding 16%)[44] due to the typically indigestible or minimally digestible nature of fish. The high crude fiber in AFP may harm animal growth. The A recipe showed the lowest crude fiber of 4.93%. Mamun, et al.[6] demonstrated that fish feed pellets derived from the *Spirulina* had protein and lipid contents of 39% and 8%, respectively, which supports excellent fish growth. Similarly, AlMulhim, et al.[45] noted that the protein fat contents are approximately 35% and 9%, respectively, derived from *Spirulina* (10%), which had the highest specific growth rate. These findings suggest that the protein and lipid levels were up to 35% and 10%, respectively.

Therefore, the A recipe at drying temperature of 110 °C was a suitable condition for the AFP development investigation using the TFT coating process due to the energy saving and the nutrient content suitability (protein, lipid, and crude fiber). The A recipe still had a weakness in the PDI property, which was expected to improve via TFT.

Optimization of coating process pellets via TFT

Table 7 presents the experimental results from the BBD, which have a DT and SEC range of 9.9–30.13 min and 0.38–0.95 kWh/kg, respectively. The desirable values were the lowest values of both responses, as the production process requires optimization to improve energy efficiency. The lowest value of DT (≈ 9 min) and SEC (≈ 0.38 kWh/kg) obtained from the process condition of Cc ≈ 1.25% (w/v), Sr ≈ 32.5 mL/min, and T ≈ 110 °C. The relationship between the productivity of coating pellets and the study parameters was displayed in Table 8. These relationships indicated the variability of variables, which were represented as equations to predict the DT and SEC values within the range. For all response surface models, the lack of fit was significant ($p \leq 0.05$), indicating that these models can explain the variance and were adequate for predicting the output. In addition, the R^2 and R^2_{adj} values of the models were greater than 0.90. The small difference in values between R^2 and R^2_{adj} (< 0.05), as illustrated in Table 8, implies that the model was appropriately specified and that most predictors were relevant in explaining the response variable. Thus, these models had an R^2 and R^2_{adj} of over 0.98, suggesting that the model fits the data without being overly complex[46]. Figure 9a and b present the relationship between the predicted DT and SEC values and experimental results, respectively. Almost all data were clustered along a straight line, indicating that the prediction DT and SEC values from both models essentially agreed with the experimental results. The regression model was statistically significant ($p < 0.05$), indicating that the independent variables collectively had a substantial effect on the DT, as well as the SEC ($p < 0.05$). The T showed the most significant effect in the linear form on DT ($p < 0.05$) and SEC ($p < 0.05$). The T largely affected the DT and SEC when the increased T caused extreme diminution of the DT and SEC, as demonstrated in Figs. 10 and 11; the lowest DT (≈ 8.2 min) and SEC (≈ 0.33 kWh/kg) occurred at 110 °C. Nanvakenari, et al.[37] reported that the T was the main effect of SEC from the fluidized bed combined with halogen and microwave drying. Similarly, Srisang, et al.[15]

Mixtures	Protein (%)	lipid (%)	Crude fiber (%)
A	37.34	11.89	4.93
B	35.51	10.08	5.72
C	33.39	9.53	5.45
Original*	26.18	5.83	-

Table 6. Nutrient content of AFP in each mixture at 110 °C. *The original recipe used fish meal as an ingredient.

Run No.	Experimental conditions			Results	
	Cc	Sr	T	DT(*)	SEC (**)
1	0.5	32.5	90	16	0.55
2	2	32.5	90	17.39	0.59
3	0.5	65	90	18.32	0.62
4	2	65	90	15.96	0.55
5	0.5	48.75	70	30.13	0.95
6	2	48.75	70	23.32	0.76
7	0.5	48.75	110	12.88	0.46
8	2	48.75	110	16.83	0.57
9	1.25	32.5	70	28.31	0.90
10	1.25	65	70	20	0.66
11	1.25	32.5	110	9.9	0.38
12	1.25	65	110	16.24	0.56
13	1.25	48.75	90	14.53	0.51
14	1.25	48.75	90	15.69	0.54
15	1.25	48.75	90	14.8	0.52

Table 7. Box-Behnken design for setting the experimental conditions and response results. (*) Drying time; (**) Specific energy consumption.

Regression Equation in Uncoded	Lack of fit	R^2	R^2_{adj}
Drying time (DT, min) 188.52 – 22.16 Cc - 0.9264 Sr – 2.748 T + 3.652 Cc*Cc + 0.009374 T*T - 0.0769 Cc*Sr + 0.1793 Cc*T + 0.01127 Sr*T	0.490	0.9938	0.9856
Specific energy consumption (SEC, kW/kg) 5.411 – 0.613 Cc + 0.02649 Sr - 0.07729 T + 0.1019 Cc*Cc + 0.000262 T*T - 0.002256 Cc*Sr + 0.005 Cc*T + 0.000323 Sr*T	0.332	0.9932	0.9842

Table 8. Regression equations in the uncoded unit.

demonstrated that the shortest DT occurs when the T was increased using a fluidized bed combined with halogen technology. The square power of concentration of chitosan (Cc^2) and drying temperature (T^2) significantly influenced DT, whereas SEC was affected by the squared terms of Cc^2, T^2, and spray rate (Sr^2). The interaction effects of Cc*Sr, Cc*T, and Sr*T were found to be statistically significant on both DT and SEC. The highest effect of interaction terms was observed in Sr*T for DT ($p < 0.05$) and SEC ($p < 0.01$). The Sr and T interaction harmed both DT and SEC; these negative correlations were confirmed by the high DT and SEC results when Sr and T declined, as represented in Figs. 10b and 11b, respectively. The lower T and the added coating solution on the surface at low Sr caused slower water evaporation, resulting in the elevation of DT and SEC. Figures 10a and 11a demonstrate that the Cc and T reductions lead to the escalated tendency of DT and SEC. Due to the solution's viscosity increasing with the addition of Cc[47], irregular substance distribution occurred on the AFP surface, contributing to agglomerate formation and negatively affecting moisture evaporation[48].

The optimal conditions aimed to minimize DT and SEC. The composite desirability was calculated by Eq. 7, confirming that these parameters provided the most favorable outcomes for both DT and SEC, as shown Fig. 12; the optimal conditions were identified at Cc ≈ 0.68% (w/v), Sr ≈ 32.5 mL/min, and T ≈ 110 °C as confirmed with the least Sect. (0.33 kWh/kg ≈ 1.19 MJ/kg) and DT (8.2 min) as shown in Table 9. The experimental results were compared with the predicted values, which revealed a few errors (< 5%), as shown in Table 10, indicating that the RSM model accurately predicted the outcomes. Nanvakenari, et al.[37] reported that the SEC of drying with the fluidized bed combined with halogen and microwave was 7.17 MJ/kg. Le, et al.[36] demonstrated that the energy consumption was 1.38 kWh for hot air drying at 110 °C. The results described in Sect. 3.1 indicated that the lowest SEC was 0.74 kWh/kg with the fluidized bed drying method. On the other hand, Palamanit, et al.[49] reported a SEC of 0.36 MJ/kg in TFT processes at a drying temperature of 50 °C, under conditions where only the effect of coating was studied. Therefore, this literature revealed higher energy consumption compared to the TFT in this study, which offered improved energy efficiency for coating and drying in AFP production. The AFP was inspected for other characterizations, including composition (XRD), microstructure (SEM), nutrient content, physical properties (WSI), mechanical properties (PDI), and antifungal activity (inhibition zone).

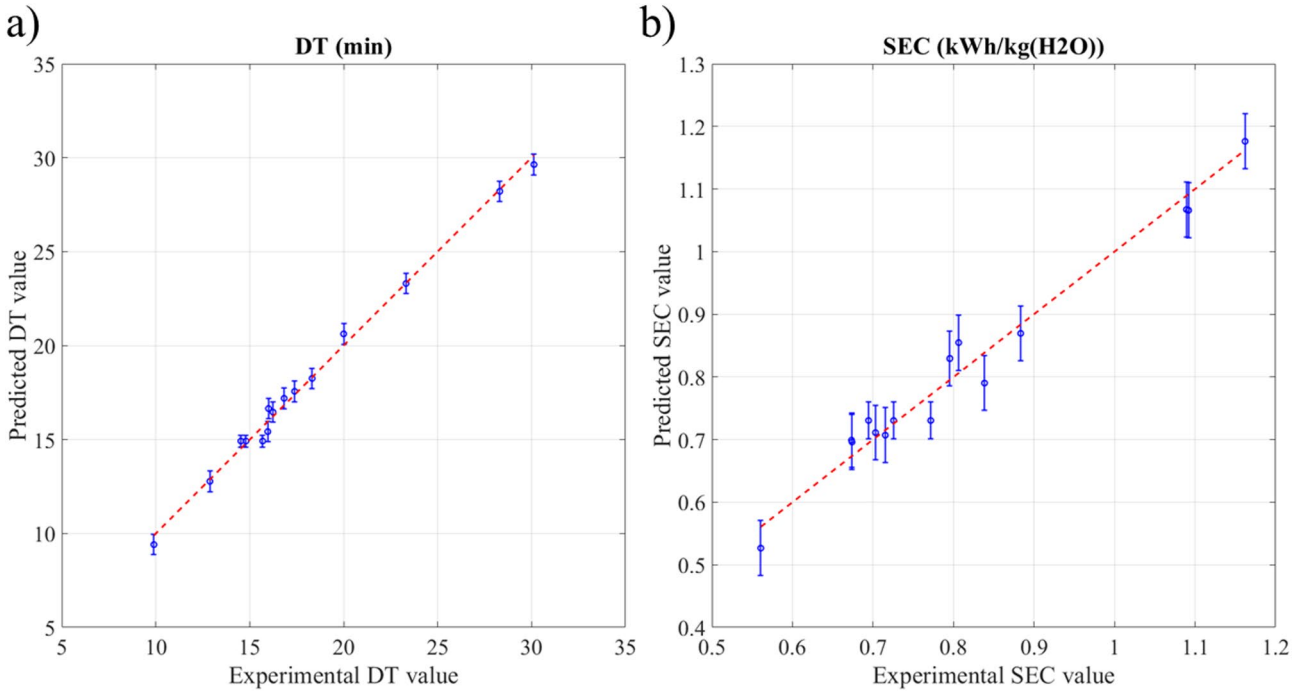

Fig. 9. Relationship between prediction and experiment values for (a) drying time (DT) and (b) specific energy consumption (SEC).

AFP characterizations after coating

Figure 13 shows the SEM results at the surface and cross-section of AFP. The microstructure of non-coating AFP exhibited the non-smooth area and some pores at the surface and the cross-section as presented in Fig. 13a and c, respectively. The porosity appearance in the AFP corresponded to the lowest PDI value as discussed in Sect. 3.1. The AFP had a smooth surface and cross-section after the chitosan coating process, as shown in Fig. 13b and d. These results were attributed to the chitosan film formation[50] and the smooth encapsulation of the AFP surface[51]. Wantat, et al.[52] reported that chitosan was coated on the fruit surface, which demonstrated that the coated surface was smoother than the uncoated one with a chitosan film. Bedade, et al.[53] reported that the application of chitosan coating resulted in a smoother and more rigid surface morphology. These findings confirmed that the chitosan coating on the AFP resulted in a smooth surface morphology, attributed to the continuous formation of the chitosan film. The XRD analysis in the AFP was used to determine the phase identification of chitosan in both coated and non-coated samples. Previous literature indicated a peak of chitosan around 20° (2θ)[54]. Figure 14 displays the XRD pattern between the coating and non-coating of AFP. The coated AFP had slightly more peak intensity at 20° than the non-coated sample due to the increased chitosan content after coating. A peak was also observed in the non-coated condition due to the AFP compositions, which consisted of shrimp shells and crab shells containing chitin and chitosan[55]. Kongtragoul and Junka[56] reported that the amount of zinc oxide on paddy increased after undergoing the zinc oxide coating process via the Top-spray fluidized bed technique.

The physical and mechanical properties of AFP were evaluated through the PDI and WSI. These indices served as key indicators of AFP quality. Figure 15a and b demonstrate the PDI and WSI comparisons at the non-coating and optimum coating conditions, respectively. The PDI average was displayed at the central line within a box, with values of 42.71% for the non-coating condition and 79.07% for the optimum coating condition, as shown in Fig. 15a. According to Khater, et al.[57], the AFP should have a PDI value greater than 71%. These results verified that the coating process under optimal conditions could significantly improve PDI beyond the established standard. The upper and lower bounds of the box are presented as 81.27% and 76.93% of the optimal coating condition, and 39.27% and 45.67% of the non-coating condition. The box plots of both conditions exhibited a narrow range and symmetrical distribution, suggesting high consistency and low variability in the experimental data. Furthermore, the highest PDI average was observed under the optimal coating condition, showing an improvement of up to 36% compared with the non-coated sample. This enhancement can be attributed to the formation of a cohesive chitosan layer on the AFP surface, which strengthened the structural integrity of the pellets. A similar trend was reported by Liu, et al.[58], who found that chitosan-coated samples exhibited higher surface hardness than uncoated samples due to the formation of a continuous and compact chitosan film. The uniform coating layer observed in our study supports this mechanism, confirming that the increase in pellet durability aligns well with previously reported findings.

The coating played a critical role in enhancing surface structure and integrity. The water solubility of AFP was a crucial attribute that indicated AFP's ability to dissolve in water[30]. Figure 15b shows the central line of the box with the WSI average at 62% for the non-coating condition and 22.81% for the optimal coating condition. The non-coating condition yielded a higher WSI value than the optimal coating condition because the chitosan

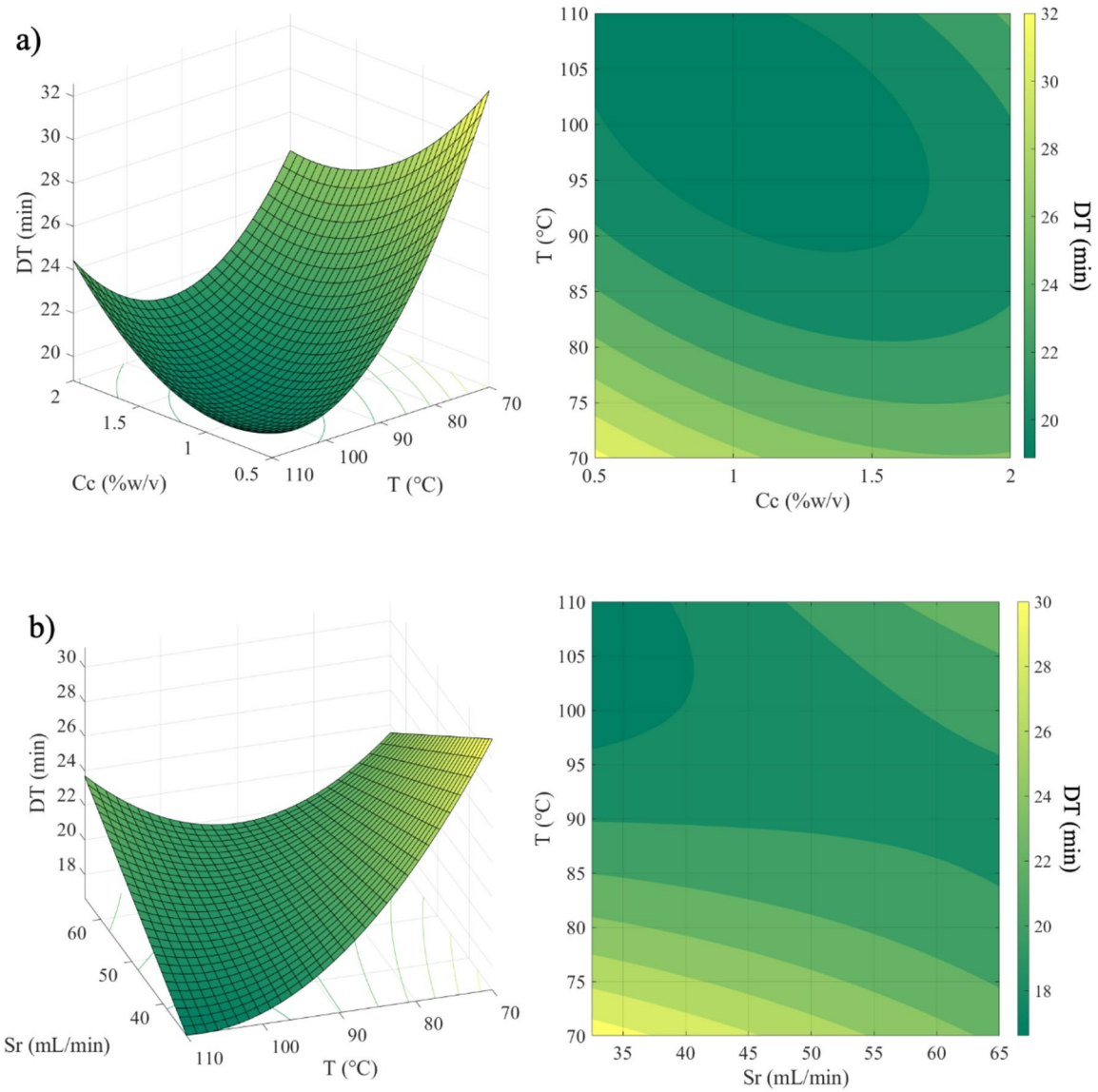

Fig. 10. Surface plots for DT in each parameter: (a) interaction between Cc and T, and (b) interaction between Sr and T.

coating enhanced the stability of AFP in water, leading to a reduced WSI value. The encapsulation of APF is attributed to the chitosan coating, resulting in slow water solubility[59]. The upper and lower bounds of the box plot for the optimal coating condition were 23.91% and 20.99%, respectively. The optimal coating condition had a narrow range in the box plot, similar to the PDI; this result implied that the AFP coating distributed excellently, likely due to the surface stabilization provided by the coating. The optimal coating condition improved the AFP surface characteristics and tended to reduce its porous morphology. The low WSI (≈ 22%) helped to prevent the excessive nutrient leaching from AFP, as stated in the study by Guo, et al.[60]. On the other hand, the non-coating condition had the wider range in the box plot, which was caused by the inconsistent porous morphology within the non-coated AFP. This research obviously demonstrated that the chitosan coating could develop the AFP's surfaces by forming a chitosan film; it reinforced the AFP's structure by reducing the pore, which led to the diminished WSI (≈ 34%) and augmented PDI (≈ 36%), respectively.

Table 11 shows a comparison of the nutrient content inside AFP at optimal coating and non-coating conditions. The coated AFP tended to reduce protein and crude fiber contents approximately 16% and 15%, respectively, as compared with the non-coated AFP. The reduction in protein content observed in this study is consistent with previous findings on the effect of acetic acid on protein structures. The use of acetic acid as a solvent for chitosan creates an acidic environment that promotes protein denaturation and partial hydrolysis. Ohishi, et al.[61] demonstrated that protein solubilization increases in the presence of acetic acid, particularly at elevated temperatures. This trend aligns with our results, where the samples exposed to 110 °C showed a more pronounced decrease in protein content. The synergistic effect of heat and acetic acid likely accelerated protein structural degradation, leading to the observed reduction. These findings confirm that the trend in our

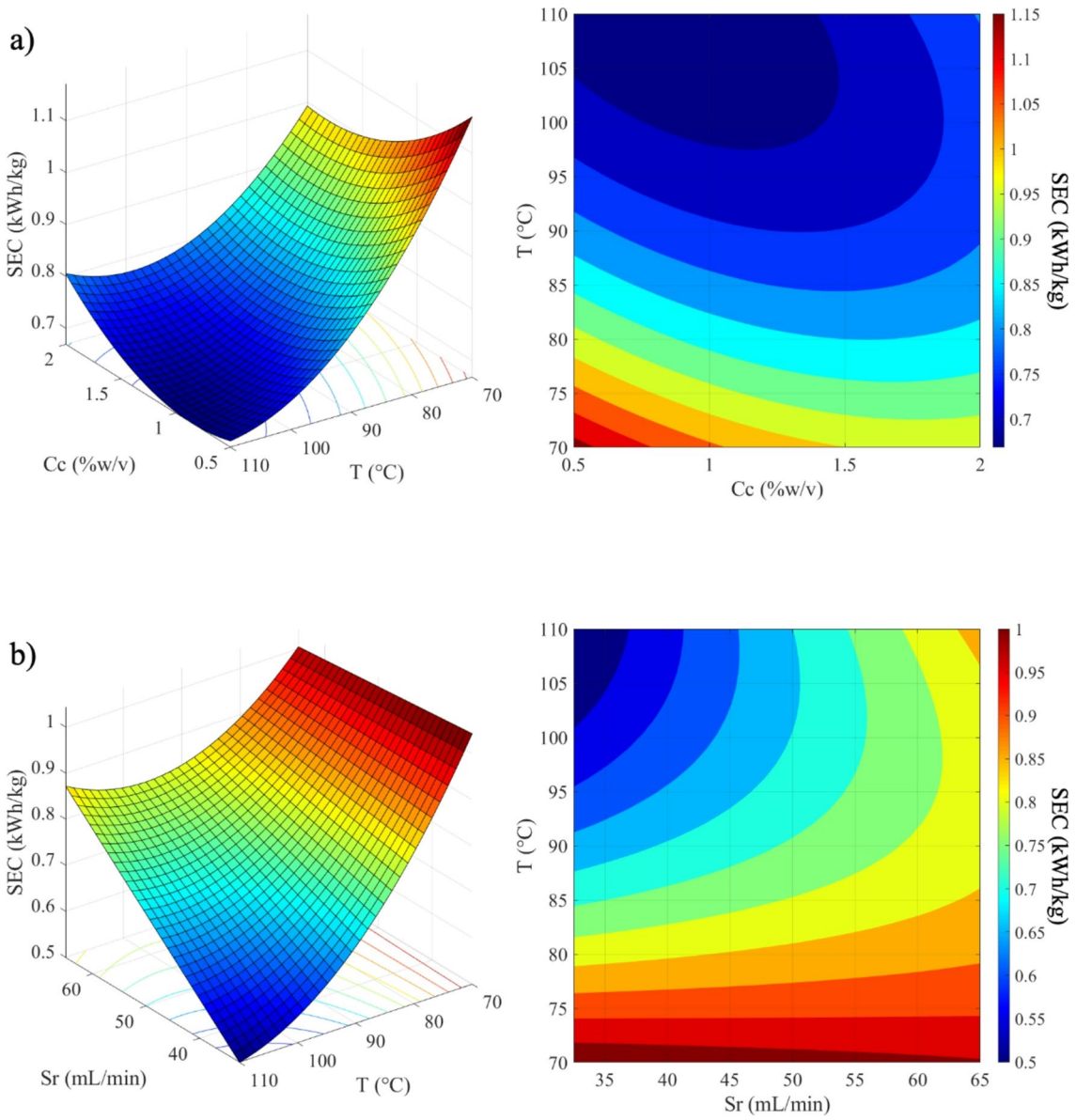

Fig. 11. Surface plots for SEC in each parameter: (a) interaction between Cc and T, and (b) interaction between Sr and T.

experimental results is in agreement with established mechanisms reported in previous studies. However, the protein and crude fiber content still met the standard criterion, while the lipid content changed only slightly. Figure 16 presents the antifungal activity (*Aspergillus spp.*) of AFP after seven days. The optimal coating condition exhibited an inhibition zone of 17.8 mm, whereas the non-coating condition showed no inhibition zone. These results indicated that the AFP had enhanced antifungal activity when coated with chitosan via TFT. Several studies have suggested that chitosan exhibits antifungal activity due to its ability to disrupt fungal cell membranes and inhibit spore germination[19,20]. The high antifungal activity enabled long-term storage. On the other hand, fungal growth was observed under non-coated conditions, attributed to the absence of protective coverage on the surface.

Therefore, the optimal coating process via TFT with chitosan solution was found to enhance the WSI, PDI, and antifungal properties of AFP. The coated AFP was characterized using SEM and XRD to confirm its surface and structural properties. Additionally, the uniformity of the chitosan coating was supported by consistent PDI and WSI values across repeated measurements, as shown in the box plots. Future studies should investigate the combination of chitosan with other additives, such as proteins, fish oil, and similar bioactive compounds, to further enhance its functional properties. Additionally, TFT should be investigated as a complex variable that influences the performance of the final product.

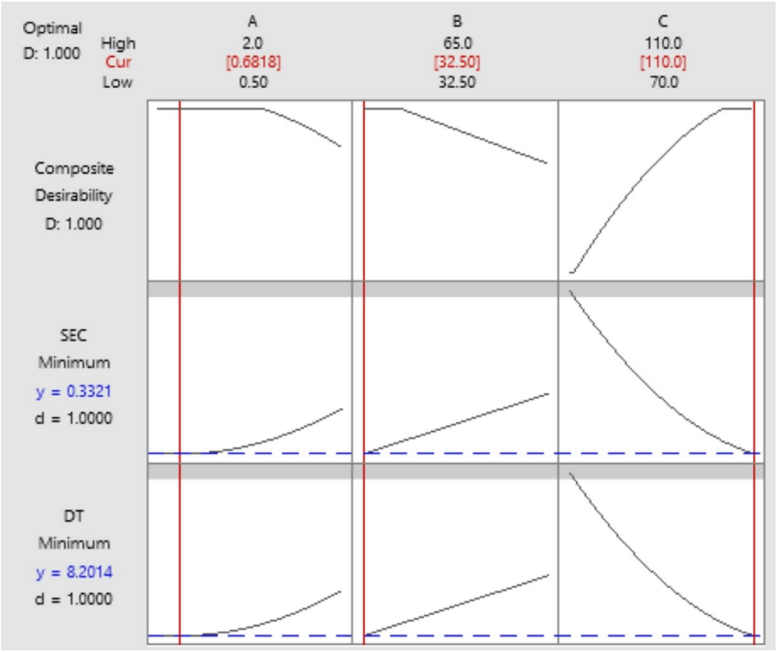

Fig. 12. The composite desirability of optimal conditions.

Response	Target	Cc	Sr	Temp	DT	SEC
DT	Min	0.68	47.6	110	8.2	-
SEC	Min	0.74	47.6	110	-	0.33
DT / SEC	Min/Min	0.68	32.5	110	8.2	0.33

Table 9. Finding the optimal condition.

	Cc	Sr	Temp	DT	SEC
RSM prediction	0.68	32.5	110	8.2	0.33
Experiments	0.68	32.5	110	8.45	0.34
Error (%)	-	-	-	3.04	3.03

Table 10. Comparison between the experiment and predicted values at optimal conditions.

Conclusion

The AFP produced from coastal waste materials, i.e., shrimp shells, crab shells, and algae, was successfully dried using an FBH at an air velocity of 10.78 m/s. Among all formulations, the A recipe exhibited the highest moisture reduction rate (134.55% d.b./min at 110 °C) and provided favorable energy consumption while retaining higher nutrient content compared with the other recipes. However, the A recipe still showed a relatively low PDI at 110 °C, prompting the application of a chitosan coating using the TFT system. The optimized coating conditions were identified as 0.68% w/v chitosan concentration, a spray rate of 32.5 mL/min, and a drying temperature of 110 °C. Under these conditions, drying time was minimized (8.2 min), and specific energy consumption was reduced (0.33 kWh/kg). The coated AFP displayed smoother surface morphology, a clearly observable chitosan phase from XRD analysis, a 36% increase in PDI, and a 34% reduction in WSI, while nutrient contents remained largely unchanged. Additionally, the coated pellets demonstrated antifungal activity against *Aspergillus spp*. These findings demonstrated the guideline for TFT application combined the chitosan usage to improve AFP qualities. Nonetheless, several limitations should be considered when these results were applied for practical production or the other utilizations. The optimized conditions were valid only within the experimental ranges (a chitosan concentration of 0.5–2% w/v, a spray rate of 32.5–65 mL/min, and a coating temperature of 70–110 °C). Any conditions were performed the outside of these ranges that may get the different results. The coating uniformity and mechanical improvement may vary depending on pellet size distribution, initial moisture content, and the composition of specific coastal-waste sources used in AFP production. In addition, although antifungal activity was observed, it was tested only against *Aspergillus spp.*, and cannot be generalized to other fungi.

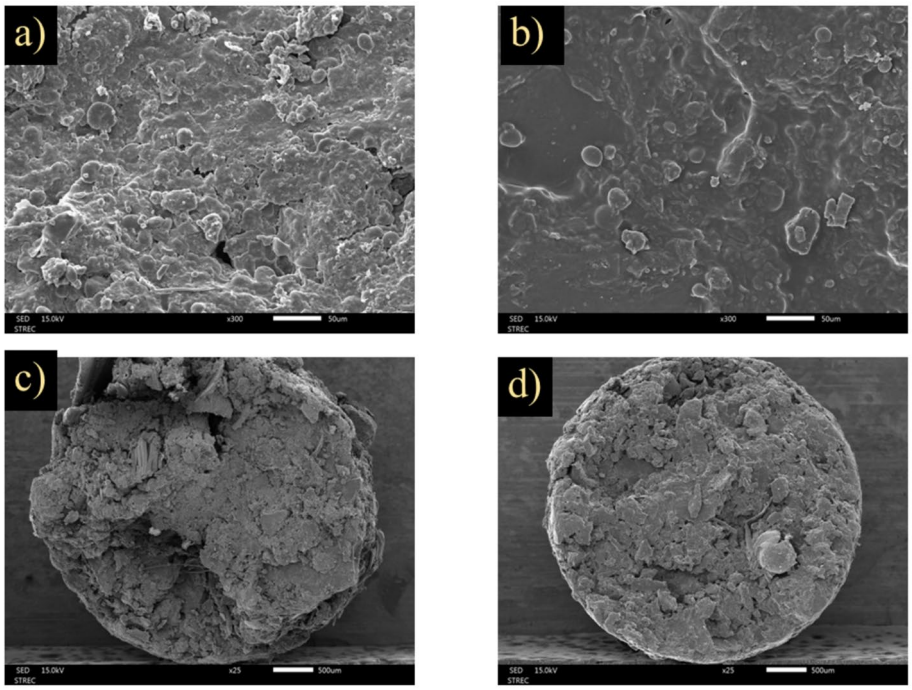

Fig. 13. SEM images of AFP at non-coating and optimum coating conditions: (a) non-coating (surface), (b) coating (surface), (c) non-coating (cross-section), and (d) coating (cross-section).

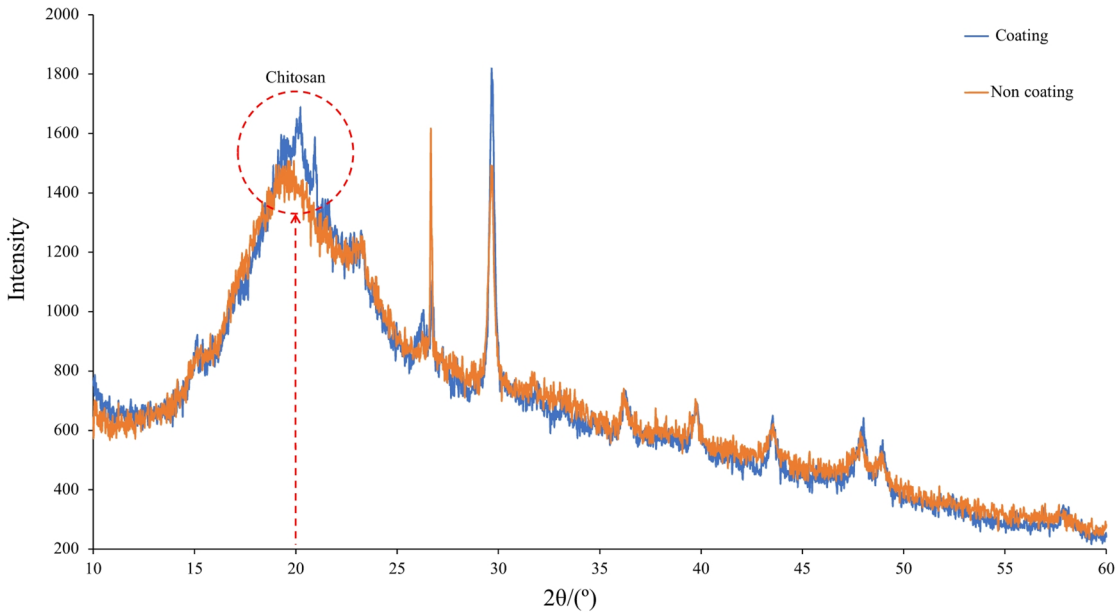

Fig. 14. XRD analysis of AFP samples in coating and non-coating conditions.

Therefore, the optimized TFT, coating with chitosan solution, offers a promising approach to enhancing AFP durability and stability. Its application should be limited to conditions comparable to those investigated in this study and verified further under industrial-scale processing.

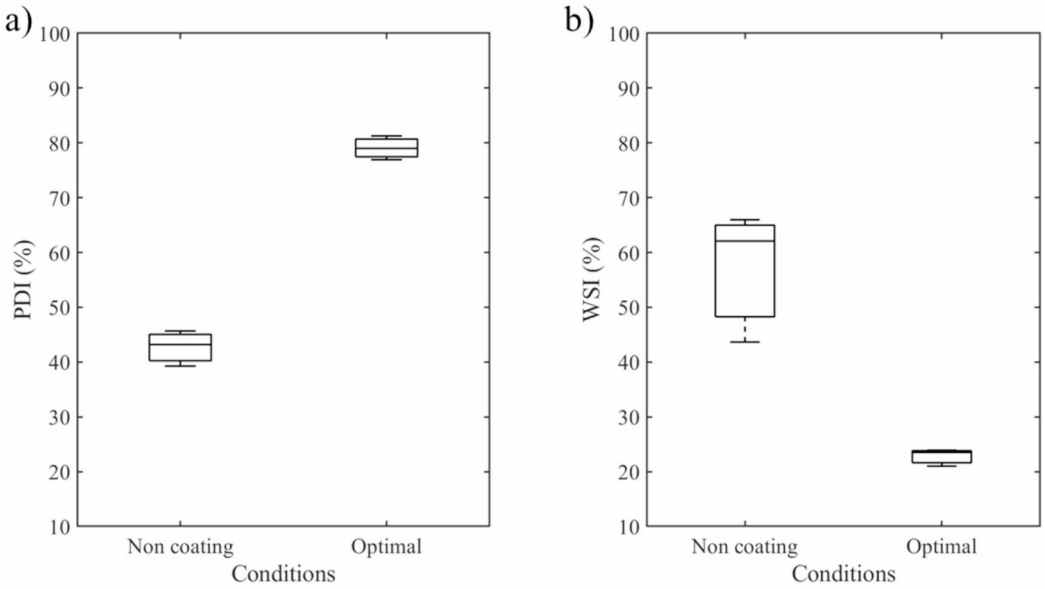

Fig. 15. The percentage of (a) PDI and (b) WSI at the non-coating and optimal coating conditions.

Conditions	Protein (%)	Lipid (%)	Crude fiber (%)
Optimal coating	29.51	9.6	7.25
Non-coating	35.17	9.51	8.57

Table 11. Nutrient content within AFP at the optimal coating and non-coating conditions.

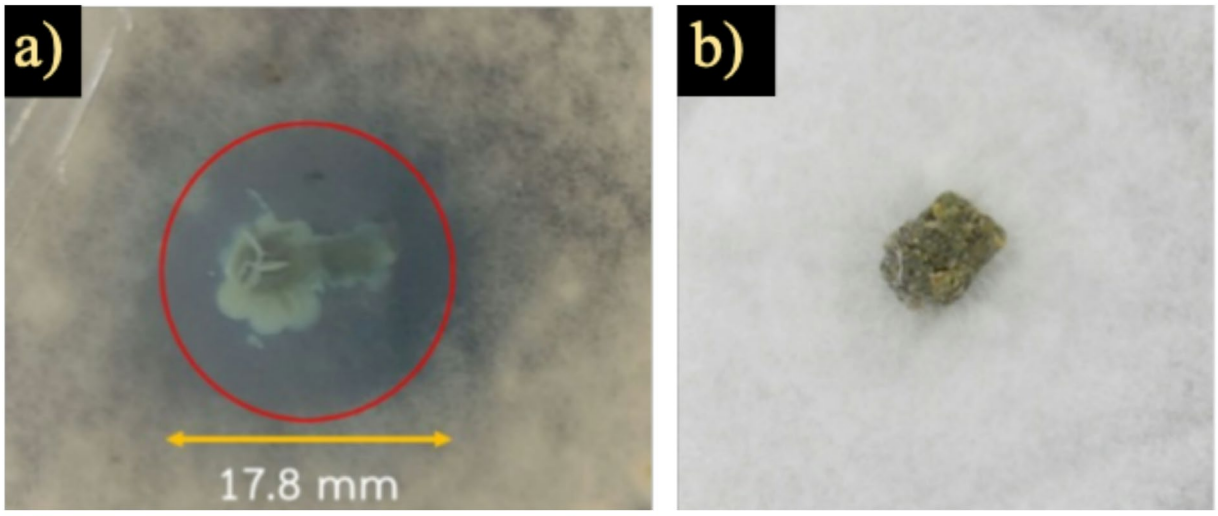

Fig. 16. The antifungal activity of the AFP 7 days: (a) coated AFP and (b) non-coated AFP.

Data availability

The datasets generated and/or analyzed during the current study are available from the corresponding author upon reasonable request.

Received: 14 October 2025; Accepted: 8 January 2026
Published online: 13 January 2026

References

1. FAO. *The State of World Fisheries and Aquaculture 2024* (FAO, 2024).
2. Eggink, K. M., Gonçalves, R. & Skov, P. V. Shrimp processing waste in aquaculture feed: nutritional Value, Applications, Challenges, and prospects. *Reviews Aquaculture*. **17** (1), e12975. https://doi.org/10.1111/raq.12975 (2025).
3. Pattanaik, S. S. et al. Characterization of carotenoprotein from different shrimp shell waste for possible use as supplementary nutritive feed ingredient in animal diets. *Aquaculture* **515**, 734594. https://doi.org/10.1016/j.aquaculture.2019.734594 (2020).
4. Sengupta, T., Mondal, A., Sagar, P., Biswas, S. & Nath, S. *Spirulina as a Dietary Supplement: Moving Toward Food Security. Ethnic Knowledge and Perspectives of Medicinal Plants* 521–533 (Apple Academic, 2024).
5. Zhang, W. et al. Effects of partial replacement of fishmeal with spirulina platensis powder and addition of spirulina platensis polysaccharide on growth, nutrition, antioxidant capacity and gut microbiota of micropterus salmoides. *Aquaculture* **586**, 740802. https://doi.org/10.1016/j.aquaculture.2024.740802 (2024).
6. Mamun, M. A. et al. Effects of spirulina spirulina platensis meal as a feed additive on growth performance and immunological response of gangetic Mystus Mystus Cavasius. *Aquaculture Rep.* **30**, 101553. https://doi.org/10.1016/j.aqrep.2023.101553 (2023).
7. Maundu, A. et al. Apparent protein digestibility and growth performance of nile tilapia (Oreochromis niloticus L.) fed on sunflower and cotton seed meal as substitutes for freshwater shrimp meal (Caridina nilotica). *Aquac. Res.* **2024** (1), 2713506. https://doi.org/10.1155/2024/2713506 (2024).
8. Roy, S. et al. A facile method for processing durable and sustainable superhydrophobic Chitosan-Based coatings derived from waste crab shell. *ACS Sustain. Chem. Eng.* **10** (14), 4694–4704. https://doi.org/10.1021/acssuschemeng.2c00206 (2022).
9. Fitriyana, D-F., Ismail, R., Bayuseno, A-P., Siregar, J-P. & Cionita, T. Characterization of hydroxyapatite extracted from crab shell using the hydrothermal method with varying holding times. *J. Renew. Mater.* **12** (6), 1145–1163 (2024).
10. Campalani, C. et al. Green extraction of Chitin from hard spider crab shells. *Carbohydr. Polym.* **345**, 122565. https://doi.org/10.1016/j.carbpol.2024.122565 (2024).
11. Olaoye, S. A., Owoseni, O. T. & Oyegoke, O. O. Effect of drying temperature on the proximate composition of soybean crude residue-base fish feed. *Int. J. Food Sci. Biotechnol.* **7** (2), 1–8 (2022).
12. Ogunnaike, A., Olalusi, A. & Orimaye, O. Effects of drying parameters on some physical properties of a dried extruded fish feeds. *J. Agricultural Eng. Technol. (JAET)* **25** (2), 18–28 (2020).
13. Ogunnaike, F. Responce surface of drying parameters on some physical properties related to floatability of extruded fish feeds. *Turkish J. Agricultural Eng. Res.* **4** (2), 178–190. https://doi.org/10.46592/turkager.1356210 (2023).
14. Carmen, P-C., Marlon, A-T., Luz, M-N., María, T-Q. & Ricardo, A-P. Influence of pre-treatment and drying process of the shrimp *(Litopenaeus vannamei)* exoskeleton for balanced feed production. *Heliyon* **9**, 6. https://doi.org/10.1016/j.heliyon.2023.e16712 (2023).
15. Srisang, N., Prachayawarakorn, S., Soponronnarit, S. & Chungcharoen, T. An innovative hybrid drying technique for parboiled rice production without steaming: an appraisement of the drying Kinetics, Attributes, energy Consumption, and microstructure. *Food Bioprocess Technol.* **14** (12), 2347–2364. https://doi.org/10.1007/s11947-021-02729-5 (2021).
16. Jafarzadeh, S., Mohammadi Nafchi, A., Salehabadi, A., Oladzad-abbasabadi, N. & Jafari, S. M. Application of bio-nanocomposite films and edible coatings for extending the shelf life of fresh fruits and vegetables. *Adv. Colloid Interface Sci.* **291**, 102405. https://doi.org/10.1016/j.cis.2021.102405 (2021).
17. Chaabani, A. et al. Optimization of vacuum coating conditions to improve oil retention in trout feed. *Aquacult. Eng.* **91**, 102127. https://doi.org/10.1016/j.aquaeng.2020.102127 (2020).
18. Junka, N. & Rattanamechaiskul, C. Optimization modeling of fluid bed drying and coating technique to control fungal growth and aflatoxin content in paddy. *J. Food Process. Preserv.* **46** (1), e16135. https://doi.org/10.1111/jfpp.16135 (2022).
19. Bhoopathy, S. et al. Curcumin loaded Chitosan nanoparticles fortify shrimp feed pellets with enhanced antioxidant activity. *Mater. Sci. Engineering: C.* **120**, 111737. https://doi.org/10.1016/j.msec.2020.111737 (2021).
20. Liu, J. et al. Synthesis, Characterization, and antifungal activity of Benzimidazole-Grafted Chitosan against Aspergillus flavus. *J. Agric. Food Chem.* **72** (19), 11185–11194. https://doi.org/10.1021/acs.jafc.4c01010 (2024).
21. Akter, M. et al. Effect of pellet-size on fish growth, feeding behaviour and natural food web in pond polyculture. *Aquaculture* **593**, 741342. https://doi.org/10.1016/j.aquaculture.2024.741342 (2024).
22. Dhurve, P., Suri, S., Malakar, S. & Arora, V. K. Multi-objective optimization of process parameters of a hybrid IR-vibro fluidized bed dryer using RSM-DF and RSM-GA for recovery of bioactive compounds from pumpkin seeds. *Biomass Convers. Biorefinery*. **14** (10), 11035–11051. https://doi.org/10.1007/s13399-022-03151-3 (2024).
23. Thinkohkaew, K. et al. Microencapsulation of probiotics in chitosan-coated alginate/gellan gum: optimization for viability and stability enhancement. *Food Hydrocoll.* **151**, 109788. https://doi.org/10.1016/j.foodhyd.2024.109788 (2024).
24. Pootthachaya, P. et al. Investigation of nutritional profile, protein solubility and in vitro digestibility of various algae species as an alternative protein source for poultry feed. *Algal Res.* **72**, 103147. https://doi.org/10.1016/j.algal.2023.103147 (2023).
25. Srisang, N., Kongbankuan, U., Jarong, N. & Srisang, S. The effect of mixture and size of fish food on the fish food qualities producing from the waste of agriculture and fishery. *Eng. Appl. Sci. Res.* **43** (0), 183–186 (2016).
26. Ao, J. et al. Impact of various drying technologies on the drying Characteristics, Physico-chemical Properties, and antioxidant capacity of walnut green husk. *Food Bioprocess Technol.* **17** (12), 4679–4693. https://doi.org/10.1007/s11947-024-03394-0 (2024).
27. de Cruz, C. R., Kamarudin, M. S., Saad, C. R. & Ramezani-Fard, E. Effects of extruder die temperature on the physical properties of extruded fish pellets containing Taro and broken rice starch. *Anim. Feed Sci. Technol.* **199**, 137–145. https://doi.org/10.1016/j.anifeedsci.2014.11.010 (2015).
28. Maikawe, J. et al. (eds) Fish Food Pellet Characteristics After Coating Using Fluidized Bed Technique. IAMBEST2023; ; King Mongkut's Institute of Technology Ladkrabang, Prince of Chumphon Campus 17/1 MOO.6 Chumkho Pathio Chumphon, Thailand. (2023).
29. Abdulhameed, A. S. et al. Insight into adsorption mechanism, modeling, and desirability function of crystal Violet and methylene blue dyes by microalgae: Box-Behnken design application. *Algal Res.* **67**, 102864. https://doi.org/10.1016/j.algal.2022.102864 (2022).
30. Wang, H. et al. Optimization of the process parameters for extruded commercial sinking fish feed with mixed plant protein sources. *J. Food Process Eng.* **44** (1), e13599 (2021).
31. Jain, S. et al. Insight into the antifungal effect of chitosan-conjugated metal oxide nanoparticles decorated on cellulosic foam filter for water filtration. *Int. J. Food Microbiol.* **372**, 109677. https://doi.org/10.1016/j.ijfoodmicro.2022.109677 (2022).
32. Mohan, K., Muralisankar, T., Jayakumar, R. & Rajeevgandhi, C. A study on structural comparisons of α-chitin extracted from marine crustacean shell waste. *Carbohydr. Polym. Technol. Appl.* **2**, 100037. https://doi.org/10.1016/j.carpta.2021.100037 (2021).
33. Cyprian, O. et al. Influence of lipid content and blanching on Capelin (Mallotus villosus) drying rate and lipid oxidation under low temperature drying. *J. Food Process Eng.* **39** (3), 237–246. https://doi.org/10.1111/jfpe.12215 (2016).
34. Kamarudin, M. S., de Cruz, C. R., Saad, C. R., Romano, N. & Ramezani-Fard, E. Effects of extruder die head temperature and pre-gelatinized Taro and broken rice flour level on physical properties of floating fish pellets. *Anim. Feed Sci. Technol.* **236**, 122–130. https://doi.org/10.1016/j.anifeedsci.2017.12.007 (2018).
35. Srisang, N., Kongbankuan, U., Jarong, N. & Srisang, S. The effect of mixture and size of fish food on the fish food qualities producing from the waste of agriculture and fishery. *Eng. Appl. Sci. Res.* **43**, 183–186 (2016).
36. Le, M. S., Hermansen, C. & Vuong, Q. V. The impact of hot air drying and vacuum drying on oat pulp quality. *Food Bioprocess Technol.* https://doi.org/10.1007/s11947-025-03862-1 (2025).

37. Nanvakenari, S., Movagharnejad, K. & Latifi, A. Modelling and experimental analysis of rice drying in new fluidized bed assisted hybrid infrared-microwave dryer. *Food Res. Int.* **159**, 111617. https://doi.org/10.1016/j.foodres.2022.111617 (2022).
38. Xing, S. et al. Partial replacement of fish meal by cottonseed protein concentrate and the effects of preconditioning water content and die temperature on pellet physical quality of extruded floating fish feed. *Anim. Feed Sci. Technol.* **304**, 115746. https://doi.org/10.1016/j.anifeedsci.2023.115746 (2023).
39. Mostafa, M. E. et al. The significance of pelletization operating conditions: an analysis of physical and mechanical characteristics as well as energy consumption of biomass pellets. *Renew. Sustain. Energy Rev.* **105**, 332–348. https://doi.org/10.1016/j.rser.2019.01.053 (2019).
40. Khater, E-S-G., Bahnasawy, A. H. & Ali, S. A. Physical and mechanical properties of fish feed pellets. *J. Food Process. Technol.* **5** (10), 1 (2014).
41. Craig, S. R., Helfrich, L. A., Kuhn, D. & Schwarz, M. H. Understanding fish nutrition, feeds, and feeding (pp. 1–6). Virginia Cooperative Extension (2017).
42. Liu, K., Frost, J., Welker, T. L. & Barrows, F. T. Comparison of new and conventional processing methods for their effects on physical properties of fish feed. *Anim. Feed Sci. Technol.* **273**, 114818. https://doi.org/10.1016/j.anifeedsci.2021.114818 (2021).
43. Jeon, D. J. & Yeom, S. H. Recycling wasted biomaterial, crab shells, as an adsorbent for the removal of high concentration of phosphate. *Bioresour. Technol.* **100** (9), 2646–2649. https://doi.org/10.1016/j.biortech.2008.11.035 (2009).
44. Nordfeldt, S., Iwanaga, I., Morita, K., Henke, L. A. & Tom, A. K. S. Influence of crude fiber in the ration on efficiency of feed utilization by dairy Cows1. *J. Dairy Sci.* **33** (7), 473–485. https://doi.org/10.3168/jds.S0022-0302(50)91925-4 (1950).
45. AlMulhim, N. M., Virk, P., Abdelwarith, A. A. & AlKhulaifi, F. M. Effect of incorporation of spirulina platensis into fish diets, on growth performance and biochemical composition of nile Tilapia, Oreochromis niloticus. *Egypt J. Aquat. Res.* **49** (4), 537–541. https://doi.org/10.1016/j.ejar.2023.08.008 (2023).
46. Singh, P., Bilyeu, L. & Krishnaswamy, K. Improving process sustainability by optimizing spray drying parameters: high oleic soymilk using response surface methodology. *Food Bioprocess Technol.* **15** (4), 833–851. https://doi.org/10.1007/s11947-021-02726-8 (2022).
47. Kienzle-Sterzer, C. A., Rodriguez-Sanchez, D. & Rha, C. K. Flow behavior of a cationic biopolymer: Chitosan. *Polym. Bull.* **13** (1), 1–6. https://doi.org/10.1007/BF00264233 (1985).
48. Song, Y., Zhou, T., Bai, R., Zhang, M. & Yang, H. Assessment of the coating quality in a top-spray fluidized bed coater: an experimental study. *Powder Technol.* **439**, 119663. https://doi.org/10.1016/j.powtec.2024.119663 (2024).
49. Palamanit, A., Prachayawarakorn, S., Tungtrakul, P. & Soponronnarit, S. Performance evaluation of top-spray fluidized bed coating for healthy coated rice production. *Food Bioprocess Technol.* **9**, 1317–1326 (2016).
50. Thakhiew, W., Devahastin, S. & Soponronnarit, S. Combined effects of drying Methods, extract Concentration, and film thickness on efficacy of antimicrobial Chitosan films. *J. Food Sci.* **79** (6), E1150–E8. https://doi.org/10.1111/1750-3841.12488 (2014).
51. Liu, D., Guo, J., Ma, J., Liang, C. & Chen, X. Effects of seed particle properties on coating in a wurster fluidized bed. *Ind. Eng. Chem. Res.* https://doi.org/10.1021/acs.iecr.3c02662 (2023).
52. Wantat, A., Seraypheap, K. & Rojsitthisak, P. Effect of Chitosan coatings supplemented with Chitosan-montmorillonite nanocomposites on postharvest quality of 'Hom thong' banana fruit. *Food Chem.* **374**, 131731. https://doi.org/10.1016/j.foodchem.2021.131731 (2022).
53. Bedade, D. K., Sutar, Y. B. & Singhal, R. S. Chitosan coated calcium alginate beads for covalent immobilization of acrylamidase: process parameters and removal of acrylamide from coffee. *Food Chem.* **275**, 95–104. https://doi.org/10.1016/j.foodchem.2018.09.090 (2019).
54. Triunfo, M. et al. Characterization of Chitin and Chitosan derived from hermetia illucens, a further step in a circular economy process. *Sci. Rep.* **12** (1), 6613. https://doi.org/10.1038/s41598-022-10423-5 (2022).
55. Pakizeh, M., Moradi, A. & Ghassemi, T. Chemical extraction and modification of Chitin and Chitosan from shrimp shells. *Eur. Polymer J.* **159**, 110709. https://doi.org/10.1016/j.eurpolymj.2021.110709 (2021).
56. Kongtragoul, P. & Junka, N. Top-spray fluidization coating of paddy rice with zinc oxide nanoparticles to reduce infection from Aspergillus Sp. *J. Food Process. Preserv.* **44** (10), e14766. https://doi.org/10.1111/jfpp.14766 (2020).
57. Khater, E.-S. G., Bahnasawy, A. H. & Ali, S. A. Physical and mechanical properties of fish feed pellets. *Int. J. Food Process.* **5**(10), 1 (2014).
58. Liu, Y., Zhu, Y., Yang, Y., Hu, S. & Jiang, W. Quality improvement of shrimp (Litopenaeus vannamei) during refrigerated storage by application of Maillard peptides/water-soluble Chitosan coating. *Food Sci. Nutr.* **10** (9), 2980–2988. https://doi.org/10.1002/fsn3.2894 (2022).
59. Lu, M. et al. Zwitterionic choline phosphate functionalized Chitosan with antibacterial property and superior water solubility. *Eur. Polymer J.* **134**, 109821. https://doi.org/10.1016/j.eurpolymj.2020.109821 (2020).
60. Guo, J., Davis, R., Starkey, C. & Davis, D. A. Efficacy of various coated materials to prevent nutrient leaching for Pacific white shrimp Litopenaeus vannamei commercial diets. *J. World Aquaculture Soc.* **52** (1), 195–203. https://doi.org/10.1111/jwas.12732 (2021).
61. Ohishi, K., Kasai, M., Shimada, A. & Hatae, K. Effect of acetic acid added to cooking water on the dissolution of proteins and activation of protease in rice. *J. Agric. Food Chem.* **51** (14), 4054–4059. https://doi.org/10.1021/jf0207169 (2003).

Acknowledgements

This work was supported by King Mongkut's Institute of Technology Ladkrabang [KREF016510].

Author contributions

Jatuphat Maikaew: Writing- Original draft, Methodology, Data curation, Project administration, Investigation-Siriwan Srisang: Methodology, Validation, Resources, Visualization, Writing- Reviewing and EditingNaruebodee Srisang: Conceptualization, Formal analysis, Investigation, Writing- Original draft, Supervision, Data curation.Supreeda Tambunlertchai: Writing- Reviewing and Editing, Software.

Funding

This research was supported by King Mongkut's Institute of Technology Ladkrabang [grant number KREF016510].

Competing interests

The authors declare no competing interests.

Additional information

Correspondence and requests for materials should be addressed to N.S.

Reprints and permissions information is available at www.nature.com/reprints.